Journal of Manufacturing Engineering, December 2009, Vol. 4, Issue 4, pp 223-232

EFFECT OF FRICTION ON BARRELLING AND COLD WORKABILITY LIMITS OF AL-4%COPPER ALLOY DURING COLD UPSET FORGING AND FEA MODELING

J Babu Rao[1], Syed Kamaluddin[2], J Appa Rao[3], M M M Sarcar[4] and N R M R Bhargava[5]

[1, 4, 5] Andhra University College of Engineering, Visakhapatnam – 530 003, India
[2] GITAM College of Engineering, Visakhapatnam – 530 045, India
[3]RVR and JC College of Engineering, Guntur – 522 019, India

ABSTRACT

Experiments were carried out to study the deformation behavior of Al-4%Cu binary alloy. Cast billets with 4%Cu by weight were upset at room temperature. Lubrication and aspect ratio (H_0/D_0) were studied as process parameters. Results show reduced barreling with lubrication. Micro hardness tests revealed a non uniform deformation with in the specimen. Micro structural features support the non uniformity in deformation from both axial and transverse direction. A 4 mm square grid, marked at the equatorial surface of sample, and deformation was studied by using an integrated PC based video recording system. Finite element analysis of deformation behavior of cold upsetting process was carried out in both dry and lubricated conditions with aspect ratios of 1.0 and 1.5. Rigid-flexible contact analysis was performed for the forming process. The comparison of various stress values obtained after 50% deformation from finite element analysis and measurement of grids using vision system were in close range.

Keywords: *Friction, Upsetting, Lubrication, Vision System, Finite Element Analysis.*

1. Introduction

Copper is one of the most important alloying elements for aluminum, because of its appreciable solubility and strengthening effect. Many commercial alloys contain copper as the major addition or the principal alloying element up to 10%. The typical applications of Al-Cu alloys are aircraft structures, rivets, hardware, truck wheels and screw-machine products [1].

Stresses in most of the metal forming processes, such as cold heading, riveting etc. are compressive in nature. Upset test at room temperature gives a representative behavior during metal forming [2-4]. Friction and lubrication affect the detailed material flow and the deformation characteristics of the work piece, the wear and fatigue failure of the tool, and the mechanical properties of the formed parts. Reduced friction lessens the stresses induced in the forming tool and prevent direct tool and work piece contact, contributing to longer tool life and better quality control [5-9]. Ring test, developed by Male and Cockcroft [10], has the greatest capability for quantitatively measuring friction under normal processing conditions.

Adoption of vision system to analyze the flow behavior of materials during upsetting has been proposed in the present work. The advantage of this method is that the experiment need not be intermittently stopped after certain deformation to measure the strains from grid. When the experiment is stopped intermittently, elastic deflections in specimen and tooling may be relieved causing inaccuracies in the next step of deformation. By use of vision system, the experiment need not be stopped during deformation process. The measurements and analysis can be done offline later. Surface strain data can be used effectively to diagnose production problems, and identify potential failure sites [11]. The non-contact and non-destructive methods can represent a real advancement for displacement, stress, strain and interfacial friction measurements. Control of these parameters may thus be exercised to understand the conditions favorable for enhanced deformation.

Present investigation makes an attempt to study the deformation behavior of cast Aluminum-4% Copper binary alloy in homogenized condition during upsetting at room temperature using vision system. Aspect ratio and friction at contact surfaces were studied as process parameters.

*Corresponding Author - E- mail: baburaojinugu@yahoo.com

© SME

2. Experimental Work

Al - 4%Cu alloy by weight was cast into 180 mm X 18 mm Φ cylindrical fingers and 200 mm X 60 mm Φ ingots. Cast ingots were homogenized at 300^0C for 24 hrs. Ring compression tests were conducted to determine the friction factor 'm' for a given set of flat platens. Standard ring compression samples of Outside Diameter (OD): Inside Diameter (ID): Height (H) = 6: 3: 2 (48: 24: 16 mm) prepared from ingots, were deformed at ram speed of 0.25 mm / sec.

Cylindrical specimens of 16 mm Φ with H_0 / D_0 ratios of 1.0 and 1.5 were machined. Specimen edges were chamfered to minimize folding. Concentric v- grooves of 0.5 mm deep were made on the flat surfaces to retain lubricant (vacuum grease) film during compression. Samples were upset by placing between the flat platens at a constant cross head speed of 0.5 mm/min in both dry and lubricated conditions, using a computer controlled servo hydraulic 100T universal testing machine. Fig. 1 shows the experimental set up of PC based on line video recording system for grid measurement during upsetting on 100t computer controlled servo hydraulic UTM.

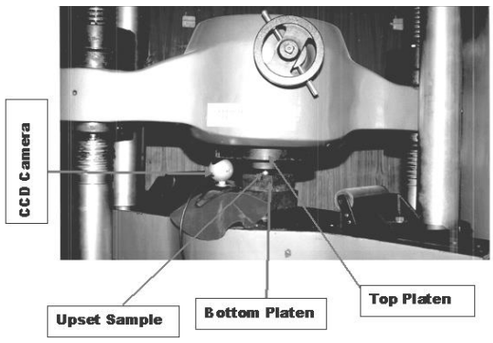

Fig. 1 Experimental Set Up

Hardness measurements were made on axial faces along the roll direction and normal direction from center to bulging end and top to center at an interval of 2 mm with 25 Pascal load (Fig. 2).

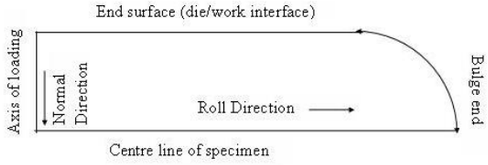

Fig. 2 Scheme of Micro Hardness Measurement for Roll and Normal Direction in a Quarter Part of Deformed Specimen

Image analyzer, (Olympus C 5060 G X 4) was used to study and record the microstructures. A PC based system with a video camera (integrated digitizing capacity, 256 color full depth 640 x 480 pixels resolution, 20 frames per second shutter speed, mounted with a magnifying lens), was used to record the images of the upsetting process. A 4 x 4 mm square grid was marked at mid height of the specimen. Online video images of grid were recorded during the upsetting process till 50% deformation. Grid distortions were analyzed offline. Images were selected at a deformation step of 5% using the software, animation shop 3.0 and are exported to paint shop pro 7.0 for further processing to get the enhanced noiseless images of high clarity.

3. Results and Discussion

3.1 Friction factor

The decrease in internal diameter of the ring compression test was plotted against deformation on Male and Cockcroft [10] calibration curve in increments of 10% deformation. From ring compression tests the friction factor 'm' for in dry condition was equal to 0.6 and that in lubricated (with vacuum grease) condition was equal to 0.3 when fit into these calibration curves with the given set of dies (same flat platens which were used for upset tests).

The end face of a dry specimen after deformation had a polished finish, while, lubricated specimen had a matt finish as shown in Fig. 3. This phenomenon indicates a low value of the coefficient of friction in lubricated condition. Similar results were observed in the works of Butler [12-14] and Tanaka et al. [15].

(a) (b) (c)

Fig. 3 Ring Test Specimens (a) Undeformed (b) 50% Deformed Lubricated (c) 50% Deformed Unlubricated

3.2 Barreling studies

The folding of material from the sides increased with increase in friction and decrease in original aspect ratio [16]. Kulkarni et al. [17] reported that the profile of the barreled surface is approximately an arc of a circle. The radius of curvature or radius of circle, R_c is plotted as a function of percent reduction in height and as a function of friction conditions for two aspect ratios, Fig. 4.

© SME

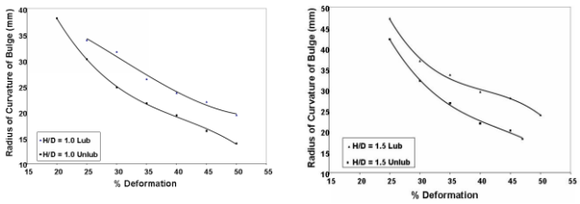

(a) (b)

Fig. 4 Reduction in Radius of Curvature (R_c) as a Function of Deformation in Lubricated and Dry Conditions for Al–4Cu alloy (a) H_0/D_0= 1.0, (b) H_0/D_0= 1.5

The value of R_c found to be decreasing with increasing deformation. R_c values were found to be smaller in dry condition compared to lubricated condition.

Three zones seem to be formed in upsetting due to inhomogeneous deformation as shown in Fig. 5. Most of the deformation takes place in zone II (center of the specimen) which causes some deformation in zone III (free end of the specimen). The material in zone I (specimen and die interface) behaves like a rigid cone penetrating the rest of the specimen Elaborate study of micro hardness distribution and microstructures revealed that the extent of deformation (or grain distortion) within the specimen at different locations were different as shown in Fig. 5. It was observed that the variation in the extent of deformation was higher in dry condition compared to lubricated condition. It was also evident that the grain distortion was more severe in the specimens with lower aspect ratio (1.0) compared to high aspect ratio (1.5) for given material. Under the same conditions of frictional constraint and aspect ratio, the severity of grain distortion was minimum at the work-die interface near the loading axis. At the center of the specimen near the loading axis the deformation was maximum, and the moderate deformation was observed at the bulge i.e. at free end.

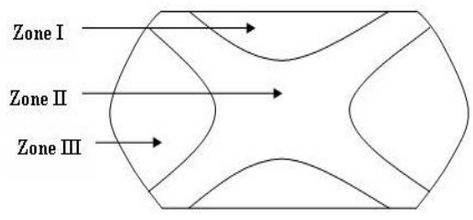

Fig. 5 Three Zones of Different Deformation Levels

3.3 Microhardness studies

The mechanical properties of the forging in terms of hardness distribution are illustrated in the Fig. 6. The high friction i.e. dry specimen showed the greatest inhomogeneity. The hardness gradient across the specimen reduced as the friction decreased, revealing a much more homogeneous structure. Theoretically, with zero friction there should be completely uniform deformation. The above results are similar to the works of Hughes et al. [18].

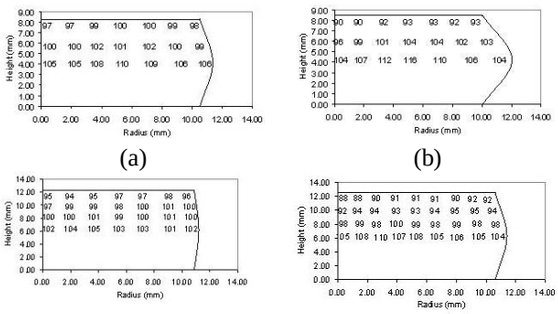

(a) (b)

(c) (d)

Fig. 6 Bulge Profile with Hardness Distribution at 50% Deformation for Al-4 Cu alloy (a) H_0/D_0=1.0 Lub, (b) H_0/D_0=1.0 Unlub, (c) H_0/D_0=1.5 Lub, (d) H_0/D_0=1.5 Unlub.

(The numbers inside the specimen profiles indicate Vickers micro hardness)

3.4 Microstructural evaluation

The microstructures of Al-4Cu alloy in as cast and homogenized condition at 300^0C for 24 hrs were presented (Fig. 7a), the partial dissolution of Cu and dispersion of the second phase ($CuAl_2$) particles which were segregated at dendritic arms [19, 20]. The presence of second phase particles in the continuous matrix phase (containing small amount of copper dissolved in aluminium) resulted in localized internal stresses which modify the plastic properties to a great extent [21, 22].

Fig. 7b shows the deformation at the die interface (zone I). The structure shows that a little amount of deformation has occurred which may be attributed to friction at the die /work piece interface. Away from the interface, i.e. at the center of the specimen the deformation is more or less uniform, figure 7c (zone II). At the bulge end the microstructure shows more pancaking, Fig. 7d (zone III), Structure also revealed skewing i.e. deformation at the angle of $15\text{-}30^0$ to the roll direction.

© SME

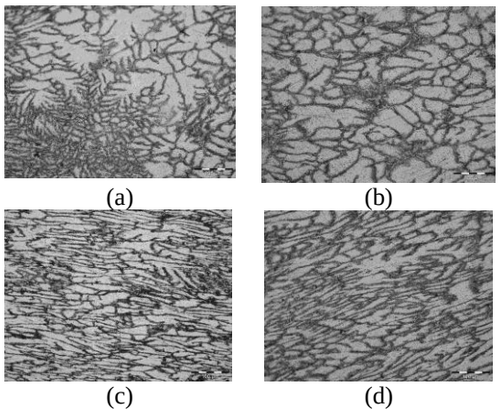

Fig. 7 Al-4Cu alloy (200 X) (a) As Cast Condition (b) Zone I (c) Zone II (d) Zone III

3.5 Flow curve

Fig. 8 (a) shows the representative plot of $\bar{\sigma}$ vs $\bar{\varepsilon}$ generated from the upsetting test data carried out at slow speed with H_0/D_0 = 1.0 using mirror finished dies. This data was treated to be material property [23]. This curve was fit into Holloman power law [24], $\bar{\sigma} = K*(\bar{\varepsilon})^n$, resulted the flow curve equations as $\bar{\sigma} = 288*(\bar{\varepsilon})^{0.31}$ for Al-4Cu alloy. This value of *K* and *n* were close to the results of Estrin, Kocks and Mecking et al. [25-27].

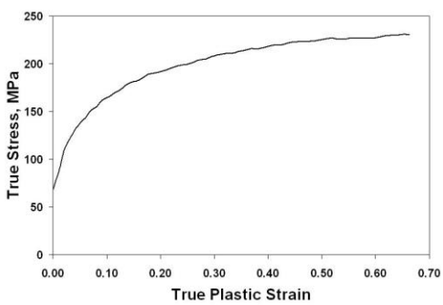

Fig. 8 True Stress vs True Plastic Strain for Al-4Cu Alloy

3.6 Experimental strain and stress analysis using vision System

Surface strains, axial strain (ε_θ) and circumferential strain (ε_z) were evaluated for the geometric mid-sectional grid of the specimens (Fig. 9) and the results were plotted in Fig. 10. Homogeneous deformation corresponds to ideal condition, that is, deformation without friction or barreling with a constant slope of $\varepsilon_\theta / \varepsilon_z$ = - 0.5. The strain paths for H_0/D_0 =1.0 in dry conditions were much steeper than H_0/D_0 =1.0 in lubricated conditions. Similar trend was evidenced for H_0/D_0=1.5, but the deviations from homogeneous were less compared to H_0/D_0=1.0.

The line with a slope $\varepsilon_\theta / \varepsilon_z$ = -0.5 on ε_θ vs ε_z plot and which intersects the ordinates at $\varepsilon_\theta \cong$ 0.3 is an estimate of a fracture line upsetting test performed on circular cylinders [28]. Though the intercept 0.3 on the ordinate may be approximately correct for steels, but may differ for material to material. Brownrigg et al [29] and H.A. Kuhn et al [30] reported these values of intercepts as 0.29, 0.32, and 0.18 for the 1045 steel, 1020 steel and 303 stainless steel respectively. In the present work these intercept value was observed to be 0.18 for Al-4Cu alloy.

The strain paths obtained from cylindrical specimens with aspect ratios 1.0 and 1.5 deviated from the slope -0.5, which represents the homogeneous deformation. It is interesting to note that all strain paths obtained from different specimens exhibited nonlinearity from the beginning to the end of the strain path. It was also observed that the slope at a point on the strain path increases as that point moves toward the end of the strain path or the fracture point. This means that at the fracture point, the incremental axial strain component was almost zero, while incremental circumferential strain component was very high. This change in the slope of the strain path has a great effect on the stress state at the surface of the specimen. The curve fitting technique was used (since the scatter in the experimental data for axial and circumferential strains) to obtain a smooth relationship between the axial strain and circumferential strain. This relationship represents the equations of the strain paths. Some of these equations for four strain paths obtained from different specimens are given in Appendix A. The ends of the strain paths represent the fracture points. Joining all the fracture points on all strain paths gives the workability limit for the alloy considered.

Fig. 9 Images of Grids Drawn at Equatorial Plane (a) Before Deformation and (b) After 50% Deformation

© SME

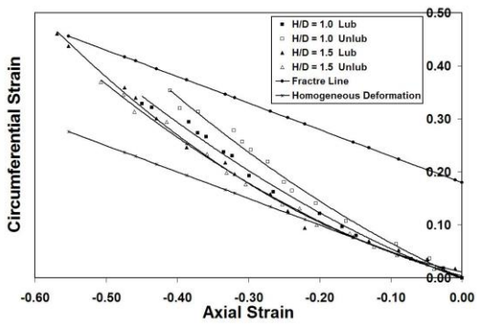

Fig. 10 Circumferential Strain (ε_θ) as a Function of Axial Strain (ε_z) at the Equatorial Free Surface

The knowledge of the experimental plastic strain history allows the experimental evaluation of stress components with the undergoing deformation (Appendix B). The magnitude of the free surface stress components for various test conditions were plotted against effective strains which were shown given in Fig. 11. In an idealized situation of uniaxial compression, the hoop stress (σ_θ), was zero and the axial stress (σ_z) was equal to the yield stress, ($\bar{\sigma}$). Under this condition the hydrostatic component of the stress, ($\sigma_H = \sigma_Z/3$) would always be compressive; a state of instability will never occur in homogeneous deformation.

Hence according to an instability theory of fracture, ductile fracture will never occur in homogenous deformation. On the other hand if the friction between the specimen and platens is more the deformation becomes non-uniform as a result of which, the barrel gets developed. The value of σ_θ was non zero and σ_H becomes less compressive and in some cases tensile. The present results referring to Fig. 11 show that with the increasing friction constraint that σ_θ increasingly tensile with continued deformation.

The σ_θ increased monotonically with continued deformation. The increase in its value was found to be more in case of dry specimens compared to the lubricated samples. On the other hand the σ_z increased in the very initial stages of deformation but started becoming less compressive immediately as barreling developed. For unfractured specimens σ_z was always compressive. However for the specimens where surface fracture occurred both σ_z and σ_H stress components became less and less compressive as deformation progressed and became tensile.

The hydrostatic stress involves only pure tension or compression and yield stress is independent of it. But fracture strain is strongly influenced by hydrostatic stress [31, 32]. As the hydrostatic stress becomes more and more tensile, a state of tensile instability will occur. In case of all the binary alloys due to presence of large portion of second phase particles, the post instability strain to fracture was small. Similar results were found with the experimental works of Edelson and Baldwin [33]. However this post instability strain to fracture can be increased by changing the microstructure via proper heat treatment as it is influenced by the grain size and inter particle distance. Such study is beyond the scope of present work.

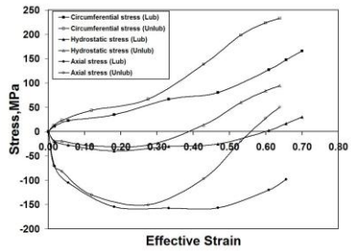

(a)

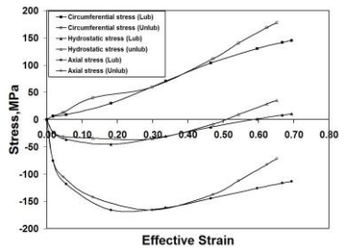

(b)

Fig. 11 Stress Components σ_θ, σ_z and σ_H as a Function of Effective Strain $\bar{\varepsilon}$ for Al– 4Cu Alloy (a) H_0/D_0 = 1.0, (b) H_0/D_0 = 1.5

3.7 Finite element modeling

Finite element analysis of deformation behavior of cold upsetting process was carried out in both dry and lubricated conditions with aspect ratios of 1.0 and 1.5. Since computers with high computational speed are now available in the market at relatively cheaper cost, the time of computation is not a major constraint for solving the problems of small sized 3-D models. Further, the tetrahedral elements can easily be accommodated in any shape and do not cause too much of distortion during deformation [34]. This reduces the number of iterations and steps to be solved. Owing to

© SME

these facts the present problem is solved using 3-D model. The analysis can also be extended to non axisymmetric problems using a full 3-D model. However, 2-D axisymmetric model is definitely advantageous for lower geometrical models in terms of computational times. In the present analysis, quarter portion of 3-D model is considered with symmetric boundary conditions.

Rigid-flexible contact analysis was performed for the forming process. For such analysis, rigid tools need not be meshed. The billet geometry was meshed with 10-node tetrahedral elements (solid 92 in ANSYS Library). Element size was selected on the basis of convergence criteria and computational time. Too coarse a mesh may never converge and too fine a mesh requires long computational time without much improvement in accuracy. The program will continue to perform equilibrium iterations until the convergence criteria are satisfied. It will check for force convergence by comparing the square root of sum of the squares (SRSS) of the force imbalances against the product of the SRSS of the applied loads with a tolerance set to 0.005. Since the tolerance value in the program is set to 0.5%, the solution will converge, only if the out of balance force is very small leading to more accurate results.

Material models selected were based on the properties of the tooling and billet materials. Due to high structural rigidity of the tooling, only the following elastic properties of tooling (H13 steel) were assigned assuming the material to be isotropic [35]. Young's Modulus E = 210 GPa and Poisson's ratio υ = 0.30. As the nature of loading is non-cyclic, Bauschinger effect could be neglected and the non-linear data was approximated to piecewise multi linear with 10 data points. The material was assumed to follow the Isotropic hardening flow rule. Suitable elastic properties were also assigned for the material chosen for analysis. As the experiments were conducted at room temperature, the material behavior was assumed to be insensitive to rate of deformation [36-38].

A 3-D, 8-noded, higher-order quadrilateral element CONTA 174 (of ANSYS library) that can be located on the 3-D solid or shell elements with mid side nodes is used. It can be degenerated to 3-7 node quadrilateral/triangular shapes. Contact surface was meshed with CONTA 174. TARGE 170 (of ANSYS library) is used to represent various 3-D target surfaces for the associated contact elements. The contact elements themselves overlay the solid elements describing the boundary of a deformable body that is potentially in contact with the rigid target surface, defined by TARGE 170 [39]. Hence a target is simply a geometric entity in space that senses and responds when one or more contact elements move into a target segment element.

3.8 Validation of FEA results

Fig. 12 shows the specimen after 50% deformation. There was zero friction at metal-die contact and no apparent bulging, the deformation can be treated as homogeneous, Fig. 12 (a). The variation in the values of radial diameter at 50% deformation obtained from finite element analysis and calculated values from volume constancy condition was 2.57 % (max) as shown in table I. This small variation may be neglected in non linear finite element analysis such as in large deformation / metal forming applications.

The increase in barreling was observed with increasing friction for aspect ratio of 1.0, Fig. 12 (b). Conical friction hills containing relatively undeformed zones were being observed as conical portions in both the cases, with the apex of cone on the axis. It was also observed that the extent of barreling decreased with increase in aspect ratio. The geometrical models (with aspect ratios 1.0 and 1.5) at 50% deformation were shown in figures 13 (a) and (b) respectively with node numbers displayed. During meshing, the element edge length was taken as 2 mm. The node number 169 for H_0/D_0 = 1.0 and node number 181 for H_0/D_0 = 1.5 respectively in geometric model corresponds to one of the grid corners drawn at mid plane of the upset sample. The stresses at these nodes were compared with the calculated values from the strains measured from grid distortions. The circumferential, axial and hydrostatic stresses after each step at these nodes were close to the calculated values from grid distortion using Machine Vision system. The results for last step i.e. at 50% deformation were tabulated in table II for the alloy under investigation. The profiles of circumferential, axial and hydrostatic stresses after 50% deformation for aspect ratio of 1.0 and 1.5 in lubricated and unlubricated conditions were shown in Fig. 14 and 15 respectively.

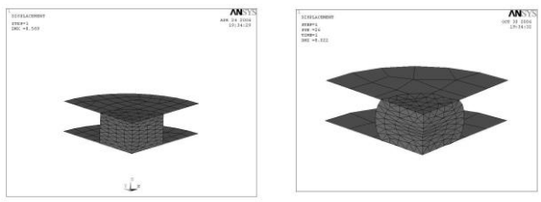

(a) (b)

Fig. 12 (a) Zero Friction, (b) Unlubricated 50% Deformation, H_0/D_0 = 1.0

© SME

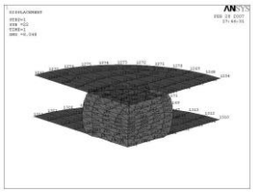

(a)

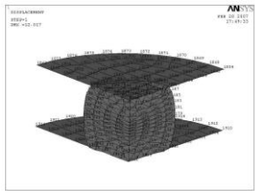

(b)

Fig. 13 Showing the Node Numbers for Geometrical Model at 50% Deformation (a) H_0/D_0 = 1.0, (b) H_0/D_0 = 1.5

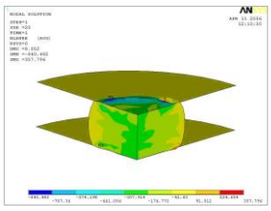

(a)

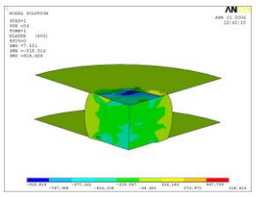

(b)

Fig. 14 (a) Hydrostatic Stress (Lubricated) (b) Hydrostatic Stress (Unlubricated). (H_0/D_0 = 1.0)

Table 1: Variation between Values of Radial Diameter after 50% Deformation at Different Friction Condition

Condition	Diameter obtained from analytical calculations, mm	Measured diameter from FEA, mm	% of Variation
H/D=1.0 (m=0)	16 X $\sqrt{2}$ = 22.628 (Assuming volume constancy)	16+ 2 X 3.234 = 22.468 (Fig. 12a)	0.71
H/D=1.0 Lub (m=0.3)	23.13	23.31 (Fig. 14a)	0.78
H/D=1.0 Unlub (m=0.6)	23.16	22.67 (Fig. 14b)	2.11
H/D=1.5 Lub (m=0.3)	22.96	23.55 (Fig. 15a)	2.57
H/D=1.5 Unlub (m=0.6)	23.31	23.03 (Fig. 15b)	1.2

Lub – Lubricated; Unlub – Un-lubricated

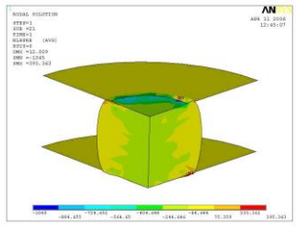

(a)

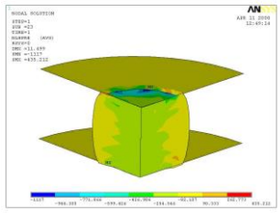

(b)

Fig. 15 (a) Hydrostatic Stress (Lubricated) (b) Hydrostatic Stress (Unlubricated). (H_O/D_O = 1.5)

Table 2: Various Stress Components at 50% Deformation Obtained From Finite Element Analysis (Numbers inside the Parenthesis Indicate the Experimental Values)

Stress, MPa →	σ_θ		σ_z		σ_H	
Condition →	Lub	Dry	Lub	Dry	Lub	Dry
H_0/D_0=1.0	167 (166)	231 (233)	-68 (-76)	51 (51)	30 (30)	94 (95)
H_0/D_0=1.5	153 (145)	183 (178)	-102 (-113)	-60 (-72)	13 (11)	37 (35)

4. Conclusions

i. The reduction in friction factor (m) from 0.6 to 0.3 was observed due to lubrication.

ii. Higher aspect ratio (H_0/D_0=1.5) with lubrication reduced barreling. This was evidenced by more uniform hardness distribution in the specimen cross section and microstructural evaluation of lubricated samples.

iii. The initial aspect ratio has considerable effect on barreling. The extent of deformation was more or less uniform for higher aspect ratio (H_0/D_0=1.5) as visualized from micro hardness and microstructural observations.

iv. Near the bulge end the microstructure revealed the pancacking.

v. Vision system allowed the reduction in experimental efforts for strain and stress analysis. Further it is noteworthy that continuous deformation helped in eliminating the elastic deflections of upsetting equipment leading to more accurate results.

© SME

vi. From the stress analysis results it is imperative that the high friction (0.6) and low aspect ratio (H_0/D_0=1.0) is the worst condition of barreling. This causes hydrostatic stress at mid plane of the cylindrical upset specimen to be tensile leading to instability there by reducing formability characteristics.

vii. The accuracy of FEA results depends on the accuracy of the input data (true stress-true strain behavior and friction factor obtained from the experiments) and friction model used in the analysis.

Appendix A: Experimental Strain Path Equations

Equations obtained by the best fit technique for the experimental strain components of different strain paths were tested by compression.

S No	Condition	Strain Path Equation
1.	H_0/D_0=1.0, Lubricated	$\varepsilon_\theta = 1.9166\ \varepsilon_z^3 + 1.8251\ \varepsilon_z^2 - 0.3132\ \varepsilon_z$
2.	H_0/D_0=1.0, Unlubricated	$\varepsilon_\theta = 1.7263\ \varepsilon_z^3 + 1.6865\ \varepsilon_z^2 - 0.4508\ \varepsilon_z$
3.	H_0/D_0=1.5, Lubricated	$\varepsilon_\theta = -0.2755\ \varepsilon_z^3 - 0.5698\ \varepsilon_z^2 - 0.4031\ \varepsilon_z$
4.	H_0/D_0=1.5, Unlubricated	$\varepsilon_\theta = -0.0836\ \varepsilon_z^3 + 0.5945\ \varepsilon_z^2 - 0.4124\ \varepsilon_z$

Appendix B: Stress Components as a Function of the Slope of the Strain Path (α)

The Levy-von Mises yield criterion can be written in terms of principal stresses as

$$\bar{\sigma} = \sqrt{3J_2} = [\sigma_\theta^2 + \sigma_z^2 - \sigma_\theta\sigma_z]^{1/2} \quad (1)$$

Because the transverse stress component σ_r is zero on the free surface. Here J_2 is the second invariant of the stress deviator. The plastic strain increment at any instant of loading is proportional to the instantaneous stress deviator, according to the Levy-Von Mises stress strain relationship: i.e.

$$d\varepsilon_{ij} = \sigma_{ij}' d\lambda \quad (2)$$

Where $d\lambda$ is non negative constant which may vary throughout the loading history.

For σ_r = 0, equation (2) yields

$$\frac{d\varepsilon_\theta}{d\varepsilon_z} = \frac{2\sigma_\theta - \sigma_z}{2\sigma_z - \sigma_\theta} \quad \text{or} \quad \frac{\sigma_\theta}{\sigma_z} = \frac{1+2\alpha}{\alpha+2} \quad (3)$$

Where $\alpha = \frac{d\varepsilon_\theta}{d\varepsilon_z}$ is a parameter which can be determined by experimental measurements of the ratio of the principal strain components in the θ and Z directions on the free surface of the specimen, Fig. 9. Substituting equations (3) and (1) gives the following expression for σ_θ and σ_z.

$$\sigma_z = \bar{\sigma}\left\{1 - \left(\frac{1+2\alpha}{2+\alpha}\right) + \left(\frac{1+2\alpha}{\alpha+2}\right)^2\right\}^{-1/2} \quad (4)$$

And $$\sigma_\theta = \sigma_z\left(\frac{1+2\alpha}{2+\alpha}\right) \quad (5)$$

By convention, compressive stresses are negative, thus the lower sign in equation (4) is used in evaluating σ_z. $\bar{\sigma}$ denotes the effective flow stress for an isotropic material for the appropriate effective strain $\bar{\varepsilon}$ at the free surface.

In terms of the principal strain increments,

$$d\bar{\varepsilon} = \frac{2}{\sqrt{3}}\left(d\varepsilon^2{}_\theta + d\varepsilon^2{}_z + d\varepsilon_\theta d\varepsilon_z\right)^{1/2} \quad (6)$$

Where, the incompressibility condition $d\varepsilon_r + d\varepsilon_\theta + d\varepsilon_z = 0$ has been used.

The effective strain at the free surface from equation (6) is given by,

$$\bar{\varepsilon} = \int_0^{\varepsilon_z} d\bar{\varepsilon} = \frac{2}{\sqrt{3}} \int_0^{\varepsilon_z} \left(1 + \alpha + \alpha^2\right)^{1/2} d\varepsilon_z \quad (7)$$

Where, the integration can be performed along the strain path provided the principal axes of the strain increment do not rotate relative to element.

The equations (4),(5) and (7), will enable us to calculate the stresses and effective strains on the geometric centre of the bulge surface (shown in Fig. 9(b)) and are identical to the equations derived by Kudo and Aoi and David et al [40, 41]. Theoretically, α may take any value between $-\infty$ and $+\infty$ but there is no real value of α for which σ_θ or σ_z would increase with out bounds. In the present experimental situation the range of α is limited to -2 to -1/2. As α

© SME

increases, the tensile stress σ_θ increases but the hydrostatic stress $\sigma_H = (\sigma_\theta + \sigma_z)/3$, becomes more and tensile which leads to a higher probability of fracture.

References

1. *Mondolfo L F (1976), "Aluminum Alloys: Structures and Properties", Butterworth and Co. Ltd, London.*
2. *Betzalel Avitzur (1977), "Metal Forming: Processes and Analysis", TMH Edition , Tata Mc Graw-Hil, Inc., New York.*
3. *Schey J A, Venner T R and Takoman S L (1982), "The Effect of Friction on Pressure in Upsetting at Low Diameter to Height Ratios", Journal of Mechanical Working Technology, Vol. 6, 23-33.*
4. *Altan T and Bonlger F W (1973), "Flow Stress of Metals and its Applications in Metal Forming Analysis", Journal of Engineering Industry, Vol. 95, 1009-1019.*
5. *Kalpakjian S (1966), "A Survey of the Feasibility of an Analytic Approach to Die Design in Closed-Die Forging", DMIC Memorandum 217, Defense Metals Information Center, Battelle Memorial Institute, Columbus, Ohio.*
6. *Kulkarni K M (1966), "The Principal Technical Development needed by the Forging Industry in the Next Decade" award winning technical paper submitted to the Forging Industry Educational and Research Foundation, Cleveland, Ohio.*
7. *Sachs G (1939), "Some Observations on the Forging of Strong Aluminum Alloys", Journal of Institute of Metals, Vol. 64, 261-283.*
8. *Hsu T C "A Study of the Compression Test for Ductile Materials", ASME Paper No. 67-WA/Met-11.*
9. *Hsu T C, and Young A J (1967), "Plastic Deformation in the Compression Test of Pure Copper", Journal of Strain Analysis, Vol. 2, 159-170.*
10. *Male A T and Cockcroft M G (1964-65), "A Method for the Determination of the Coefficient of Friction of Metals under Conditions of Bulk Plastic Deformation", Journal of Institute of Metals, Vol.93, 38-46.*
11. *Babu Rao J (2007), "Studies on Flow Behaviour of Aluminium, Aluminium–Copper and Aluminium–Copper-Magnesium alloys during Cold Upsetting Using Vision System", Ph. D Thesis, Andhra University, India.*
12. *Butler L H (1957), "The Effects of Lubricants on the Surface Appearance of Aluminum after Plastic Deformation", Metallurgia, Vol. 55, 63-66.*
13. *Butler L H (1960), "Surface Conformation of Metals Under High Nominal Contact Pressures", Metallurgia, Vol. 61, 167-174.*
14. *Butler L H (1959-1960), "The Effect of Interposed Lubricants on the Surface Deformation of Metals during Plastic Working", Journal of Institute of Metals, Vol. 88, 337-343.*
15. *Tanaka E, Semoto S, and Wantanabe S (1965), "Relation between Surface Appearance and Coefficient of Friction in Compressive Deformation of Metals", Tohoku University Science Report Research Institute, Series A, Vol. 17, 208-218.*
16. *Unksov E P (1961), "An Engineering Theory of Plasticity", Butterworth, London.*
17. *Kulkarni K M and Kalpakjian S (1969), "A Study of Barreling as an Example of Free Deformation in Plastic Working", Journal of Engineering for Industry, Vol. 91, 743-754.*
18. *Hughes D A, Kassner M E, Stout M G and Vetrano J S (1998), "Metal Forming at the Center of Excellence for the Synthesis and Processing of Advanced Materials", Journal of Metals, Vol. 50, 16-21.*
19. *Joseph R Davis (1993), "Aluminum and Aluminum Alloys", ASM Specialty Hand book, ASM International, Materials Park, OH.*
20. *Samaras S N and Haidervenopolons G N "Evaluation of Micro Structure during Extrusion Processing of Aluminum Alloys", Materials laboratory, Dept. of Mechanical and Industrial Engineering, School of Engineering, University of Thessaly, Volos, Greece.*
21. *Takeji A B E, Shigeru N A, Gaki and Tetsuya Akase (1985), "Material Inhomogenity and Surface Roughening during Plastic Deformation", Bulletin of JSME, Vol. 28(236), 251.*
22. *Shevakin J U F and Tsypin M I (1997), "The Curves of Plastic Flow and Deformation Strengthening of Some Solid Solution on the Basis of Copper", Advanced Performance Materials, Vol. 4, 233-238.*
23. *Gouveia B P P A, Rodrigues J M C and Martins P A F (1996), "Fracture Predicting in Bulk Metal Forming", International Journal of Mechanical Sciences, Vol. 38, 361-372.*
24. *Samuel K G (2006), "Limitations of Hollomon and Ludwigson Stress-Strain Relations in Assessing the Strain Hardening Parameters", Journal of Phys. D: Appl. Phys, Vol. 39, 203-212.*
25. *Estrin Y (1996), "In Unified Constitutive Laws for Plastic Deformation", Academic Press, London.*
26. *Kocks U F (1976), "Laws for Work-hardening and Low-temperature Creep", Journal of Engineering Material Technology, Vol. 98, 76-85.*
27. *Mecking H, Nicklas B, Zarubova N and Kocks U F (1986), "Kinetics of Flow and Strain-hardening", Acta. Metall, Vol. 29, 1865 1875.*
28. *Samantha S K (1975), "Effect of Friction and Specimen Geometry on the Ductile Fracture in Upset", Institute of Engineering Materials and Technology, Transactions of ASME, 14-20.*
29. *Brownrigg A, Duncan J L and Embury J D (1979), "Free Surface Ductility of Steels in Cold Forging", Internal Report, Mc. Master University, Hamilton, Ontario, Canada.*
30. *Kuhn H A, Lee P W and Erturk T (1973), "A Fracture Criterion for Cold Forming", Journal of Engineering Materials Technology, Transactions of the ASME, 213-218.*

© SME

31. *George E Dieter (1988), "Mechanical Metallurgy", McGraw-Hill Book Company, London.*

32. *Brozzo P, Deluca B, and Rendina R, (1972), "A New Method for the Prediction of Formability Limits in Metal Sheets", Sheet Metal Forming and Formability: Proceedings of the 7th Biennial Conference of the International Deep Drawing Research group.*

33. *Edelson B and Baldwin W (1962), "The Effect of Second Phases on the Mechanical Properties of Alloys", Transactions of the ASM, Vol. 55, 230-250.*

34. *Wu W T, Jinn J T, and Fischer C E, Scientific Forming Technologies Corporation, Chapter15.*

35. *http://www.matweb.com*

36. *Lee C H and Kobayashi S (1973), "New Solutions to Rigid-Plastic Deformation Problems Using a Matrix Method", Journal of Eng. Ind. (Trans. ASME), Vol. 95, 865.*

37. *Taylan Altan and Dan Hannan (2002), forgFing: Prediction and Elimination of Defects in Cold Forging using Process Simulation –The Engineering Research Center for Net Shape Manufacturing.*

38. *Zeinkiewiez O C (1984), "Flow Formulation for Numerical Solution of Forming Processes", in J.F.T. Pittman et al. (Eds), Numerical Analysis of Forming Processes, New York, Wiley, 1- 44.*

39. *Ansys 8.0 reference manual.*

40. *Kudo H and Aoi K (1967), "Effect of Compression Test Condition Upon Fracturing of a Medium Carbon Steel – Study on Cold – Forgeability Test; Part II", Journal of the Japan Society of Technical Plasticity, Vol. 8, 17-27.*

41. *David W Manthey, Daeyong Lee and Rebecca M Pearce (2005), "The Need for Surface Strain Measurement", Metal Forming Magazine.*

Nomenclature

Symbol	Meaning
H_0	Initial height of the cylindrical sample
D_0	Initial diameter of the cylindrical sample
H_0 / D_0	Aspect ratio
h_0	Original height of the square grid
h_i	Current height of the square grid
w_0	Original width of the square grid
w_i	Current width of the square grid
K	Strength coefficient
n	Strain- hardening exponent
α	Strain ratio (slope of the strain path)
ε_z	Axial strain
ε_θ	Circumferential strain
$\bar{\varepsilon}$	Effective strain
$\bar{\sigma}$	Effective stress
σ_r	Radial stress component
σ_z	Axial stress component
σ_θ	Circumferential stress component
σ_H	Hydrostatic stress $[(\sigma_r + \sigma_\theta + \sigma_z)/3]$

Acknowledgements

The authors thank the AICTE, New Delhi for their financial support under AICTE – CAYT scheme (File No:1-51/FD/CA/(19) 2006-2007) and also the Departments of Metallurgical and Civil Engineering, AU College of Engineering, Andhra University Visakhapatnam for providing necessary support in conducting the experiments.

© SME